PROCEEDINGS OF SCIENCE

Cosmic-Ray Physics (Direct, CRD): Rapporteur Talk

Stefano Gabici[a,*]

[a] *Université Paris Cité, CNRS, Astroparticule et Cosmologie, F-75013 Paris, France*

E-mail: gabici@apc.in2p3.fr

In this paper, I summarise the results presented during the sessions on Cosmic-Ray Physics (Direct, CRD) at the 38th International Cosmic Ray Conference.

38th International Cosmic Ray Conference (ICRC2023)
26 July - 3 August, 2023
Nagoya, Japan

*Speaker

PoS(ICRC2023)030

1. Introduction

In a very well known (and beautiful) review article published in 2005, Hillas [1] reported on the status of the research on Galactic cosmic rays. Figure 1 on that review showed the spectrum of cosmic rays as measured by various experiments. In commenting that plot, Hillas wrote that *a single component of cosmic rays appears to extend from below* 10^{10} eV *to at least* 10^{16} eV *in proton energy. To a good approximation a uniform spectrum in rigidity,* $R^{-2.69}$*, consistent with the expectations of a simple ('test particle') shock acceleration model, is quite acceptable.*

The observed spectrum of cosmic rays $n_{CR}(R)$ is shaped by the interplay of acceleration at sources (i.e. injection of cosmic rays in the interstellar medium) and transport in the interstellar turbulent magnetic field (i.e. escape from the Galaxy). The former determines the rate at which cosmic rays are released by Galactic cosmic accelerators and their energy (or rigidity) spectrum, $q_{inj}(R)$, while the latter determines the confinement time of cosmic rays in the Galaxy, $\tau_{esc}(R)$. At equilibrium, one would expect $n_{CR}(R) \sim q_{inj}(R) \times \tau_{esc}(R)$ (see [2] for a more extended discussion). If $n_{CR}(R) \propto R^{-2.69}$ is a pure power law and one wants to avoid excessive fine tuning, then also $q_{inj}(R)$ and $\tau_{esc}(R)$ must both be power laws. As diffusive shock acceleration theory suggests that $q_{inj} \propto R^{-\alpha}$ with $\alpha \gtrsim 2$ (e.g. [3]), the escape time will scale as $\tau_{esc}(R) \propto R^{-\delta}$ with $\delta \sim 2.69 - \alpha \lesssim 0.69$. This is a very remarkable result, with important consequences. Indeed, if the escape time scales with rigidity/energy as a single power law then, very likely, the same mechanism is responsible for the confinement of cosmic rays of all energies *from below* 10^{10} eV *to at least* 10^{16} eV.

This rather straightforward scenario based on pure power laws turned out to be inadequate to fit the precision cosmic ray data collected by PAMELA [4] starting from 2006 and then by AMS-02 since 2011 [5]. The new picture that emerged from such data, and was later corroborated by data from other missions such as CALET [6], DAMPE [7], and ISS-CREAM [8], revealed that the spectra of cosmic ray nuclei *cannot be described by pure power laws*, but exhibit a sequence of spectral breaks. These observational findings will be reviewed in Section 2 below, together with possible theoretical interpretations.

The discovery of breaks in the spectra of nuclei [9–17], together with the difference in the observed slope of the proton and helium spectra [10–12], the rise of the positron fraction with particle energy [18], the surprisingly hard spectrum of antiprotons [18], the prominent break observed in the electron spectrum at $\sim$ 1 TeV [19], the flattening of the B/C ratio at large particle rigidities [20, 21], and the unexpected flatness of the ^{10}Be/^{9}Be isotopic ratio [22] are probably the most surprising results obtained in the past $\sim$15 years of direct studies of the cosmic radiation. However, it is not clear yet whether some adjustments to the standard picture for cosmic ray origin will suffice to explain all of these data, or if a radical change of paradigm is required (see [2] for an extended discussion). Therefore, both options must be explored.

After discussing breaks in the spectra of nuclei in Sec. 2, I will review isotopic studies (Sec. 3), measurements of electrons/positrons/antiprotons (Sec. 4), studies on low energy ($\sim$MeV) cosmic rays (Sec. 5), and a number of other findings that do not fit in any of the previous Sections (Sec. 6). I will then conclude in Sec. 7.

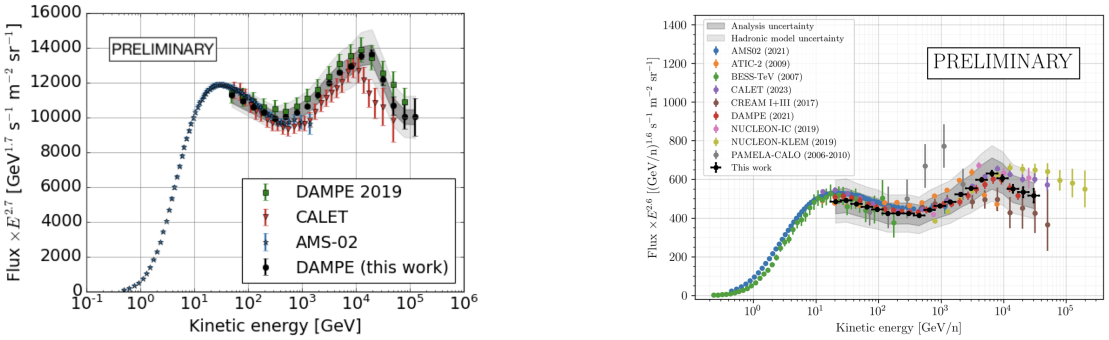

(a) **(b)**

Figure 1: Spectrum of cosmic ray protons (a) and helium (b) as a function of the kinetic energy per nucleon measured by various experiments. Figure from [10].

2. Nuclei

2.1 Protons and helium nuclei: how to explain the different spectral slopes?

Figure 1 shows a compilation of measurements from various experiments of the proton and helium spectrum of cosmic rays. Above particle energies of $\sim$ 20 GeV/nucleon, where the effects of solar modulation are negligible, spectra are clearly not single power laws, but exhibit two spectral breaks. For protons, a spectral hardening appears at $\sim$200 GeV, and a steepening at $\sim$1 TeV (see left panel of Fig. 1). The same qualitative behaviour is observed also in the energy spectrum of helium (right panel of Fig. 1), but in that case the breaks are observed at slightly different (lower) values of the energy per nucleon. This is indeed not surprising, as the acceleration and transport of relativistic particles depend uniquely on how charged particles move in a magnetic field of strength B, i.e., on their Larmor radius, which is defined as $r_L = R/B$. Therefore, spectral features present in the spectra of different species are expected to align when spectra are plotted as a function of particle *rigidity* rather than energy per nucleon. This is illustrated in Fig. 2.

Before discussing the possible origins of such breaks, it is interesting to compare the slopes of

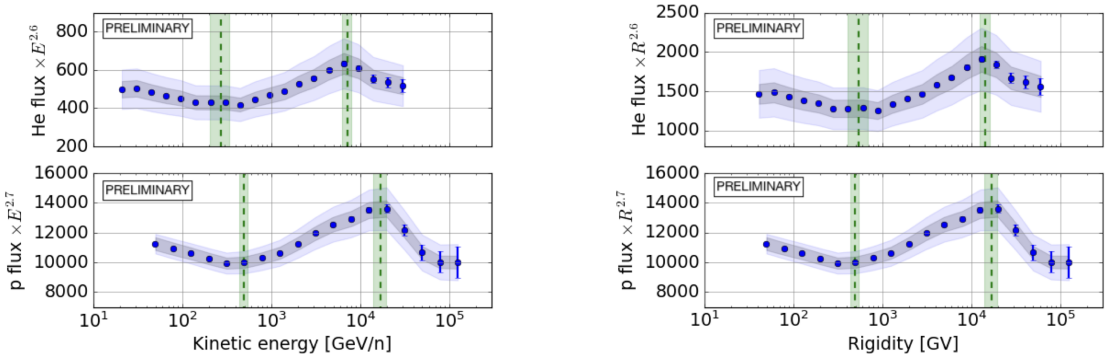

Figure 2: Spectra of cosmic ray helium (top) and protons (bottom panels) measured by DAMPE and plotted as a function of energy per nucleon (left panels) and rigidity (right panel). Figure from [10].

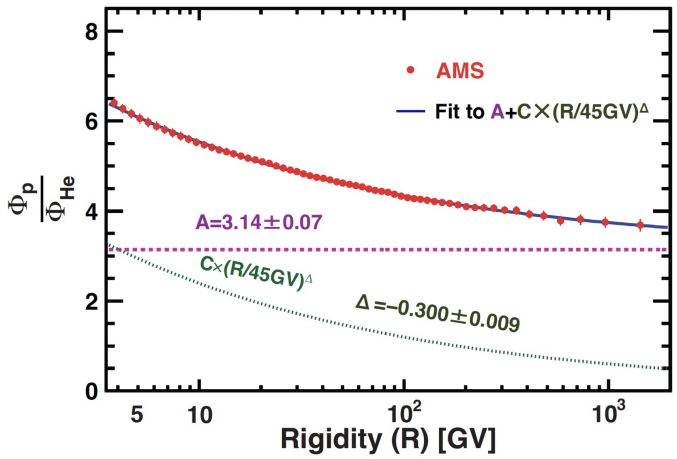

Figure 3: Ratio of the proton over helium spectrum as a function of rigidity as measured by AMS-02 after 11 years of data acquisition. Figure unpublished and presented at ICRC by [11].

the spectra of protons and helium nuclei. This can be done with the help of Fig. 3 (from [11]), which shows that the ratio of the proton-over-helium spectra is a mildly decreasing function of rigidity. Explaining why the proton spectrum is slightly steeper than the helium one is still an open issue. Various possibilities have been suggested (see [23] for a review), but all of them face difficulties. At least three scenarios can be envisaged:

1. One might invoke a physical process that affects helium nuclei and not protons (or vice-versa). A natural candidate is spallation of helium nuclei in the interstellar medium. The problem with this scenario is that the effectiveness of spallation increases with the atomic mass number. Therefore, the amount of spallation required to modify the helium spectrum would likely result in an excessive amount of spallation of heavy nuclei.

2. Another possibility is to assume that proton and helium nuclei are accelerated in a different way. This, however, would conflict with the well motivated belief of *universality* of acceleration mechanisms (for example, spectra of particles accelerated via diffusive shock acceleration are invariably power laws with hslope close to $\propto R^{-2}$, regardless of environmental conditions).

3. Finally, protons and helium nuclei might be accelerated in different places, characterised by different metallicities (e.g. helium rich versus helium poor environments) or different atomic ionisation states (e.g. helium can be mainly ionised in some phases of the interstellar medium and mainly neutral in others, and in the latter case it would not be accelerated being insensitive to the presence of magnetic fields). Environmental effects might slightly change the slope of spectra of particles accelerated at shocks, and this might explain the different slopes. The need of fine tuning is the weak point of such scenario.

2.2 A break (hardening) at 200 GV: two regimes of cosmic ray transport

Let us now discuss cosmic ray nuclei heavier than H and He. Remarkably, the spectral feature observed at 200 GV is present also in the spectra of heavies. This is shown in Fig. 4, were spectra

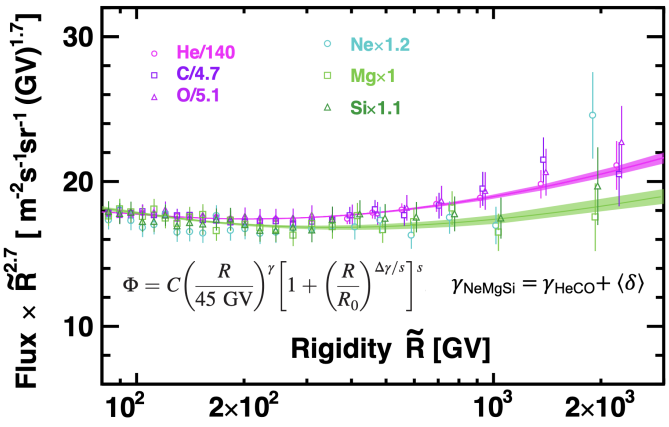

Figure 4: Renormalised spectra of He, C, O, and Ne, Mg, Si as a function of rigidity as measured by AMS-02 after 11 years of data acquisition. Figure unpublished and presented at ICRC by [11].

of several primary species are shown as a function of rigidity. After being rescaled, all spectra roughly overlap and follow the same behaviour. They invariably show the hardening at 200 GV.

There are two possibilities to explain the hardening: either a break is present in the spectrum of cosmic rays injected in the Galaxy, $q_{inj}(R)$, or a break is present in the cosmic ray confinement time in the Galaxy, $\tau_{esc}(R)$. The measurement of the spectrum of *secondary*[1] light nuclei, such as Li, Be, and B, can be used to distinguish between these two scenarios [15, 24]. Such spectra are shown in Fig. 5, together with the spectra of some primaries. Remarkably, also the spectra of secondaries hardens at a rigidity which is similar to that where also the spectra of primaries hardens. However, the hardening is twice more pronounced for secondaries, and this makes it possible to distinguish between the two possible interpretations of the break.

Consider first the case where the injection spectrum of cosmic ray primaries (for example C) is characterised by a break at a rigidity R_b, while the cosmic ray confinement time in the galaxy is a pure power law in rigidity. For rigidities below R_b the injection spectrum is $q_{inj}(R) \propto R^{-\gamma}$, while for larger rigidities it is $q_{inj}(R) \propto R^{-\gamma+\Delta}$, where γ and Δ are both positive. On the other hand, the confinement time is $\tau_{esc} \propto R^{-\alpha}$ for all rigidities, with $\alpha > 0$. As seen in Sec. 1, the equilibrium spectrum of cosmic ray primaries in the Galaxy is $n_{CR} \sim q_{inj} \times \tau_{esc}$. Secondary species (such as B) will be produced via spallation and their spectrum will be very close to that of primaries, $q^{sec}_{inj}(R) \propto n_{CR}(R)$, which gives an equilibrium spectrum in the Galaxy equal to $n^{sec}_{CR} \sim q^{sec}_{inj} \times \tau_{esc}$. Therefore, the equilibrium spectrum of primaries (secondaries) scales as $n_{CR} \propto R^{-\gamma-\alpha}$ ($n^{sec}_{CR} \propto R^{-\gamma-2\alpha}$) and $n_{CR} \propto R^{-\gamma+\Delta-\alpha}$ ($n^{sec}_{CR} \propto R^{-\gamma+\Delta-2\alpha}$) in the low and high rigidity regime, respectively. One can see that the spectral index decreases above the break by the same amount Δ for both primaries and secondaries, and therefore this scenario is falsified by data.

Let us now repeat exactly the same reasoning for the scenario where the injection spectrum is a pure power law $q_{inj}(R) \propto R^{-\gamma}$ and the escape time hardens from $\tau_{esc} \propto R^{-\alpha}$ to $\tau_{esc} \propto R^{-\alpha+\Delta}$ above a rigidity R_b. Under these conditions, the equilibrium spectra of primaries and secondaries scales exactly as in the previous case in the low rigidity domain, while at large rigidities they

[1]Cosmic ray particles are named *primary* if they are accelerated out of the interstellar medium, and *secondary* if they are the result of spallation of heavier cosmic ray nuclei following their collisions with interstellar matter.

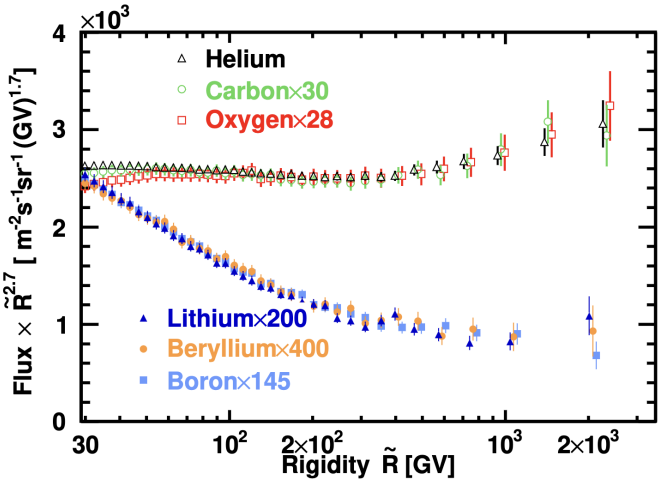

Figure 5: Spectra of primary (He, C, and O) and secondary (Li, Be, and B) nuclei measured by AMS-02 and plotted as a function of rigidity. Figure from [15].

scale as $n_{CR} \propto R^{-\gamma+\Delta-\alpha}$ and $n_{CR}^{sec} \propto R^{-\gamma+2\Delta-2\alpha}$, respectively. The hardening in the spectrum of secondaries is twice more pronounced (2Δ instead of Δ) than that in the spectrum of primaries, in agreement with observations. This demonstrates that the spectral break at ~200 GV is due to the properties of particle transport.

The change in the slope of the cosmic ray confinement time is interpreted as a transition between two regimes of transport. At low energies, where most particles reside, the stream of cosmic rays escaping the Galaxy triggers a plasma instability (called streaming instability) that amplifies pre-existing magnetic turbulence. This in turn enhances the efficiency of the scattering of cosmic rays off (*self-generated*) magnetic irregularities and decreases their confinement time in the Galaxy. At large energies, the scarce number of cosmic rays reduces the effectiveness of the instability, and cosmic rays scatter off the pre-existing (*external*) turbulence. Even though no prediction for the spectrum of cosmic rays was made, such change in the regime of transport was hypothesised in the very early days of cosmic ray transport studies [26]. Remarkably, the transition from scattering off self-generated to external turbulence was expected to take place at $O(100$ GV), which is very close to what has been observed! A modern and elegant discussion of this issue can be found in [25].

2.3 A break (softening) at 10 TV: which origin?

A spectral steepening is observed in the cosmic ray proton and helium spectra at a rigidity of $\sim$ 10 TV (see Fig. 1, 2, and [9, 10, 12, 27]). To date, its presence in the spectrum of heavier elements cannot be established due to poor statistics at high energies. A striking feature of the break is its sharpness (see left panel of Fig. 6), which is difficult to be reproduced by models (see curves in the right panel of the same figure).

As for the break at 200 GV, also the origin of the steepening at 10 TV can be ascribed either to a break in the injection spectrum of cosmic rays (see e.g. [29]) or to transport/escape in/from the Galaxy (see e.g. [30]). Unfortunately, at the moment, it is not clear which scenario provides a

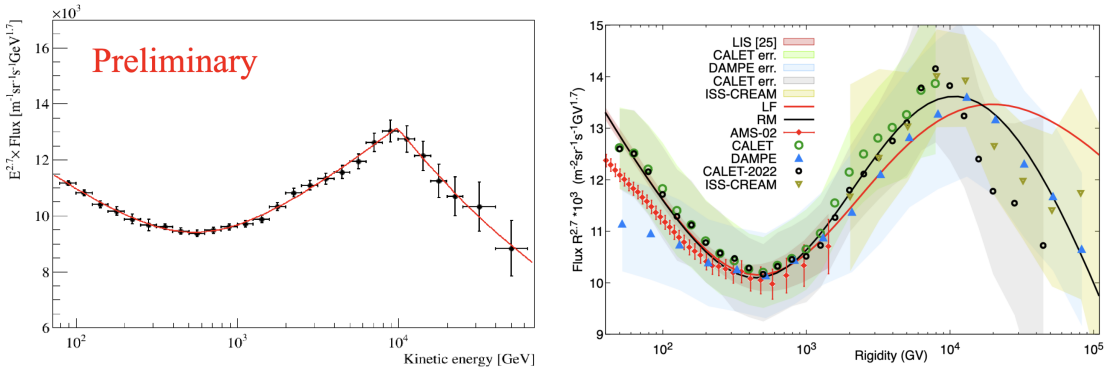

Figure 6: Spectrum of cosmic ray protons as measured by CALET (left) and various experiments (data points in the right panel). In the right panel, model fit to data are also shown (black and red lines). Figures from [9] (left) and [28] (right panel).

better explanation of data.

The recent detection of this additional spectral feature confirms that the spectrum of cosmic rays, as well as the explanation of its origin, is more complex than we thought.

2.4 Primaries versus secondaries: three groups of cosmic rays

Numerical codes aimed at modelling the transport of energetic particles in the Galaxy (e.g. [31, 32]) are customarily used to fit the observed spectra of different cosmic ray species. The results obtained running these codes can be used to determine if a given element is primary or secondary. In fact, the output of the fit provides the fraction of each element abundance having a primary or secondary origin.

Approximate estimates of such fractions can be obtained without running propagation codes, but simply combining spectral measurements of different cosmic ray species. To do that, the spectrum of a given element i can be written as the sum of a primary contribution plus a secondary one:

$$\Phi_i(R) = c_p \times \Phi_p(R) + c_s \times \Phi_s(R) \quad (1)$$

where $\Phi_p(R)$ and $\Phi_s(R)$ are proxies for the spectra of pure primary (p) and pure secondary (s) elements, respectively, and c_p and c_s are fit coefficients. In order for this method to work, the primary element p should not be too far from the element i in the periodic table, and should be characterised by a primary fraction very close to 1. For light elements, oxygen is a good choice as a reference primary, because of its large abundance, while for secondaries one may take boron. By using these proxies, it was possible to show, for example, that a small fraction of Carbon (at the 10-20% level) is of secondary origin [16], in broad agreement with more accurate estimates obtained using transport codes. For heavier elements, a convenient choice is Silicon as a proxy for primaries, and Fluorine for secondaries.

For a number of elements, such as for example Nitrogen, Sodium or Aluminum, the primary and secondary components are found to be of comparable magnitude (see Fig. 7). This shows that cosmic rays can be divided into three categories: elements which have a (predominantly) primary, secondary or mixed origin. This is illustrated in a very convincing way in Fig. 8, where the

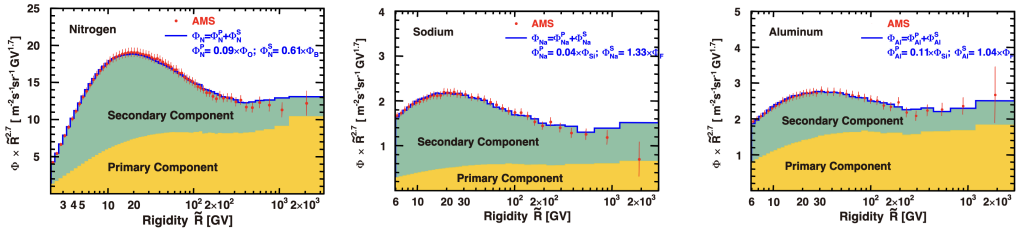

Figure 7: Spectrum of cosmic ray Nitrogen (left), Sodium (center), and Aluminum (right). The yellow and green shaded regions show the primary and secondary component for each element. Figure from [17].

(renormalised) spectra of many different elements are shown. The spectral similarities are evident, and allow to classify He, C, O, Fe, Ne, Mg, Si and S as primaries, Li, Be, B, and F as secondaries, and N, Na, and Al as mixed origin elements. Of course, this simplified approach cannot replace accurate studies based on transport codes, but shows that a lot of information can be extracted from data based only on very simple and reasonable assumptions.

2.5 The B/C (and B/O) ratio

The measurement of the B/C ratio plays a central role in cosmic ray physics. Cosmic ray Boron is entirely secondary, and is predominantly produced by spallation of cosmic ray Carbon (Oxygen is also a major contributor), which has a number density in the Galaxy equal to n_C, with atoms in the interstellar gas of density n_{ISM}. The rate at which Boron is produced in these interactions is $q_{\rm B} \approx n_C n_{ISM} \sigma_{\rm C\to B} v$ where $\sigma_{\rm C\to B}$ is the spallation cross section and v the velocity of Carbon nuclei. The equilibrium density of cosmic ray Boron is then $n_B \sim q_B \times \tau_{ISM}$, where τ_{ISM} is the time spent by cosmic rays in the interstellar medium before leaving the Galaxy. The amount of matter traversed by cosmic rays in a time τ_{ISM} is called grammage and is $\lambda \sim m_p n_{ISM} v \tau_{ISM}$. It

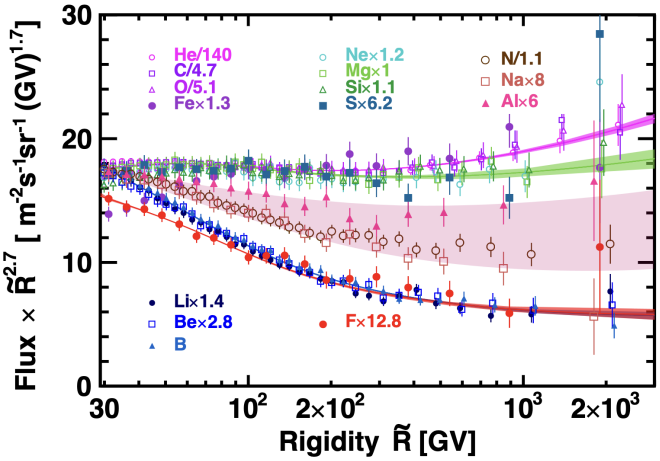

Figure 8: Renormalised spectra of (mostly) primary (upper data points: He, C, O, Fe, Ne, Mg, Si, S), secondary (lower data points: Li, Be, B, F), and mixed origin (intermediate data points: N, Na, and Al) cosmic rays. Figure from [17].

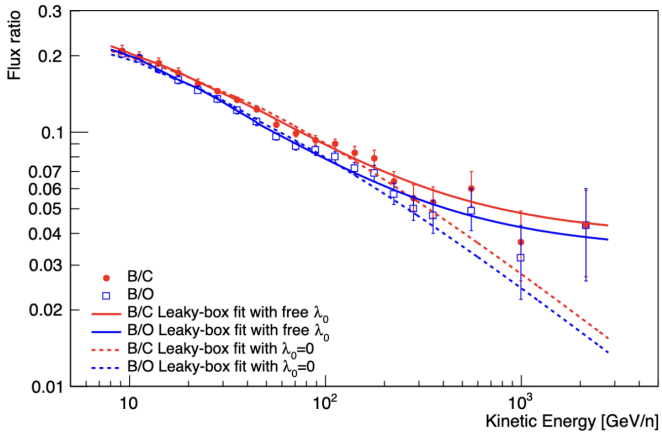

Figure 9: B/C and B/O ratios as measured by CALET. Figure from [21].

follows that the grammage is tightly connected to the cosmic ray B/C ratio that can be expressed as:

$$\frac{n_B}{n_C} \approx \lambda \frac{\sigma_{\mathrm{C}\to\mathrm{B}}}{n_C} \tag{2}$$

The expression above is a brutal oversimplification (see [2, 47] and references therein for a more accurate approach) but illustrates how the measurement of the B/C ratio can be used to infer the grammage and therefore the residence time of cosmic rays in the Galactic disk. In fact, considering the Galaxy (disk and halo of thickness h and H, respectively) as a box of mean gas density $\bar{n} = n_{ISM}(h/H)$, and reminding that the cosmic ray diffusive escape time is $\tau_{esc} \sim H^2/D$ (D is the cosmic ray diffusion coefficient) one can see that the grammage can be expressed as:

$$\lambda \approx \sigma_{ISM} v \left(\frac{H}{D}\right) \tag{3}$$

where $\sigma_{ISM} = m_p n_{ISM} h$ is the surface density of the gas in the disk of the Galaxy. Measuring the grammage is equivalent to measuring the ratio between the cosmic ray diffusion coefficient and the height of the Galactic cosmic ray halo.

The declining behaviour of the grammage (roughly a power law in energy per nucleon $\lambda \propto E^{-s}$ for energies smaller than $\approx$ 1 TeV/n) shows that higher energy cosmic rays are less confined than lower energy ones. The DAMPE and CALET collaboration reported on measurements of the B/C ratio at very high energies (beyond 1 TeV/n) [20, 21]. The B/C (as well as the B/O) ratio clearly flattens at the highest measured energies and the corresponding grammage can be tentatively described by a scaling $\lambda = aE^{-s} + \lambda_0$, with $\lambda_0 \gtrsim 1$ g/cm^3.

The additional (flat) component in the grammage can be explained in (at least) two ways: either the transport of cosmic rays becomes energy independent at energies larger than $\sim$ 1 TeV, or cosmic rays accumulate the grammage inside (or in the vicinity of) their sources. The first scenario would require that the spatial diffusion of cosmic rays of all energies exceeding $\sim$ 1 TeV is characterised by a constant mean free path of:

$$l_{m.f.p.} = \frac{3D}{v} \approx 30 \left(\frac{D}{10^{30}\mathrm{cm}^2/\mathrm{s}}\right) \mathrm{pc} \tag{4}$$

where D is the cosmic ray diffusion coefficient at multi-TeV energies. Remarkably, the mean free path is of the same order of magnitude of the coherence scale of the turbulent magnetic field in the interstellar medium. On the other hand, the latter scenario would require cosmic rays to remain trapped within sources for a time:

$$\tau_{trap} \approx 2 \times 10^5 \left(\frac{\lambda}{1 \text{ g/cm}^3} \right)^{-1} \left(\frac{n_{ISM}}{1 \text{ cm}^{-3}} \right)^{-1} \text{yr} \tag{5}$$

where I assumed that the density inside the cosmic ray sources is equal to $4 \times n_{ISM}$ (which is appropriate for a gas compressed at a strong shock). It is interesting to note that such a timescale is roughly comparable to the lifetime of a supernova remnant. At the moment, both scenarios are possible and appealing, and should be further investigated.

3. Isotopic studies

The abundance of the short lived radionuclide ^{10}Be in cosmic rays carries precious information about the transport of cosmic rays in the halo (see e.g. [2] and references therein). ^{10}Be is produced in spallation of cosmic rays with interstellar matter and, thanks to its short lifetime (τ_{rad} is about 2 Myr) is an ideal *cosmic ray clock*. The ratio between the abundance of ^{10}Be and its stable companion ^{9}Be provides the most stringent constraint on the cosmic ray confinement time in the Galaxy. A brutal way to understand why this is the case consist in ignoring all (sometimes important, indeed) complications and consider only the main difference between these isotopes: one is stable and the other is not. ^{10}Be and ^{9}Be are produced in the Galactic disk at a rate q_{10} and q_9, respectively. These rates can be computed as we measure spectra of heavier cosmic ray nuclei (the most relevant being C and O) as well as nuclear cross sections. Then, stable isotopes of ^{9}Be leave the Galaxy after an escape time τ_{esc}, while ^{10}Be isotopes decay in a time τ_{rad}. It follows that the abundance ratio can be written (very brutally!) as:

$$\frac{n(^{10}\text{Be})}{n(^{9}\text{Be})} \approx \left(\frac{q_{10}}{q_9} \right) \left(\frac{\gamma \tau_{rad}}{\tau_{esc}} \right) \tag{6}$$

where τ_{rad} has been multiplied by the Lorentz factor of ^{10}Be γ to account for time dilation effects. Most remarkably, the combined measurement of the ^{10}Be/^{9}Be and the B/C (see Equations 3 and 2) ratios can be used to constrain both the cosmic ray diffusion coefficient D and the height of the cosmic ray halo H (and not only their ratio).

The AMS-02 collaboration presented recent data (still unpublished) that extend the measurement of the ^{10}Be/^{9}Be ratio up to an energy of $\gtrsim$ 10 GeV/n, which is about one order of magnitude larger than what was available before [14]. The energy dependence of the ratio was found to be much flatter than expected (see data points in Fig. 10). When data are compared with the prediction of the transport models by Evoli and collaborators [33], it is found that a good fit would require a surprisingly large value of the cosmic ray halo, i.e., H significantly larger than 12 kpc. A large value of H implies that also D should be quite large (in order to fit the B/C ratio), in tension with the (lower) values required to explain the low level of anisotropy of cosmic rays up to very large energies.

A possible solution for this tension was presented in [34], where a scenario was investigated where the cosmic ray diffusion coefficient in the Galactic disk D_d is smaller with respect to that

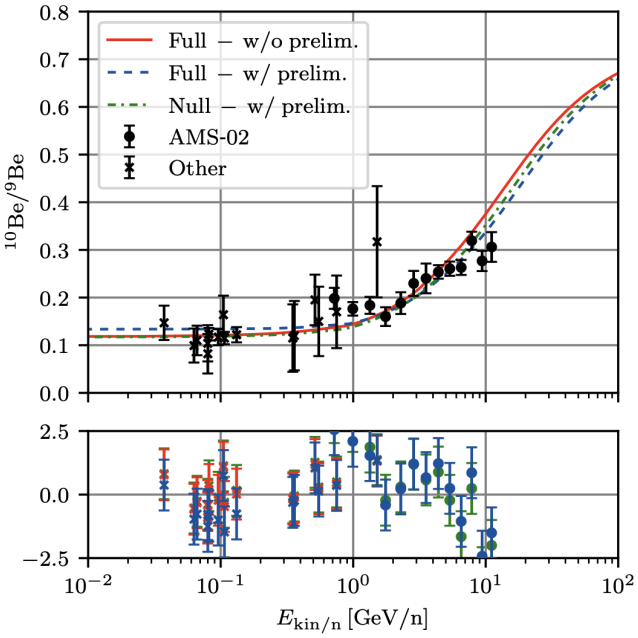

Figure 10: ^{10}Be/^{9}Be ratio as measured by AMS-02 (data points) compared with models assuming that the cosmic ray diffusion coefficient in the disk is smaller than that in the halo (curves). Figure from [34].

in the cosmic ray halo D_h. A possible reason for that is that pockets of reduced cosmic ray diffusivity might exist around cosmic ray sources (which are located in the disk), due to a plasma instability (streaming instability) triggered by the streaming of cosmic rays escaping from their sources. Whether such pockets play or not a role in cosmic ray transport on Galactic scales is a matter of debate [35]. A good fit to a preliminary set of AMS-02 data is obtained when D_d is suppressed by a factor of about 5 with respect to D_h (see Fig. 10). The ratio ^{10}Be/^{9}Be is sensitive to the diffusion coefficient especially at low particle energies, as for large energies ^{10}Be behaves as a stable isotope due to time dilation (see Eq. 6).

Finally, other isotopic anomalies were discussed, including:

1. Recently, claims on the presence of a primary component in the spectrum of Lithium (^{7}Li) where made [36]. However, as noticed by Maurin and collaborators [37], the need for primary Lithium disappears when revised spallation cross sections are adopted. Finally, the AMS-02 collaboration reported a preliminary measurement of the cosmic ray ^{7}Li/^{6}Li ratio whose explanation does not require the presence of primary Lithium.

2. Anomalies were also reported for the ratios D/^{3}He [38] and ^{3}He/^{4}He [39]. Most of deuterium and ^{3}He isotopes are produced in spallation of ^{4}He, which is characterised by a comparatively small cross section. As a consequence, D and ^{3}He are generated within a correspondingly large distance from the Solar system, and explaining the anomalies might require a spatially inhomogeneous behaviour of cosmic ray transport [40].

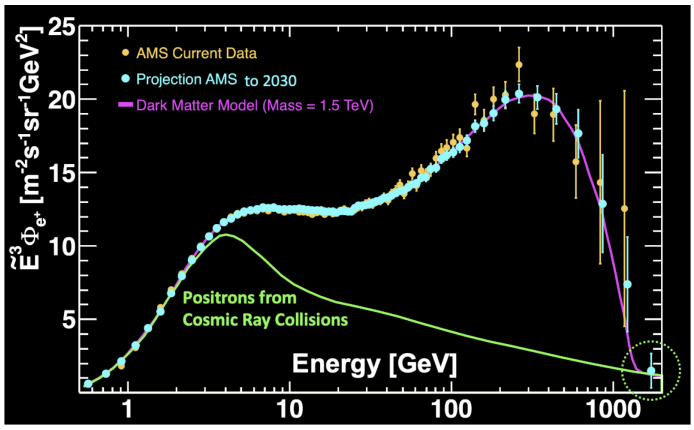

Figure 11: Cosmic ray positron spectrum as measured by AMS-02 (yellow data points). A prediction of AMS-02 observations extrapolated to 2030 is also shown (cyan data points). Predictions have been computed by assuming a dark matter scenario for positron production (magenta line), plus a secondary contribution coming from cosmic ray collisions in interstellar matter (green line). Figure from [18].

4. Electrons, positrons, antiprotons

One of the most debated issues in cosmic ray physics is the origin of the so called positron excess. Positrons are naturally produced in inelastic interactions between cosmic ray protons and interstellar matter. This is a guaranteed source of positrons whose intensity can be estimated with good accuracy from the knowledge of the spectrum of cosmic ray protons. It is represented as a green curve in Fig. 11. Data points (the yellow ones) in the same figure clearly show that an additional component is required. The two scenarios which are most often invoked ascribe to origin of the excess either to positron acceleration in astrophysical sources (sometimes referred to as *new* sources) or to dark matter decay [18].

In fact, a long time ago Harding and Ramaty [41] (in a proceeding paper from the ICRC that took place in Moskow in 1987) speculated on the existence of a pulsar contribution to the cosmic ray positron intensity, when only vague hints of a possible rise in the positron spectrum could be derived from data.

A possible way to distinguish between the pulsar and dark matter scenario would be to extend the measurements of positrons to larger energies. The cyan (simulated) data points in Fig. 11 show what AMS-02 will be able to do after collecting data until 2030. Data points have been simulated by assuming that the positron excess is due to dark matter decay (magenta line in the figure), i.e., the spectrum terminates quite abruptly with an exponential cutoff. If this is indeed the case, AMS-02 might be able to se the recovery in the spectrum at multi-TeV energies due to the positron component produced in cosmic ray interactions in the interstellar medium (see Fig. 11). It would be interesting, however, to simulate also the alternative scenario, as the spectrum of positrons produced by pulsars is expected to be a *broken power law* rather than a power law plus cutoff. In that case, the spectrum of the positrons making the excess would extend to much larger energies and, as a consequence, it would be most likely impossible to identify the interstellar component of positrons.

The total electron spectrum (total meaning electrons plus positrons) has been measured up to the TeV and multi-TeV domain by CALET [19], DAMPE [7], and H.E.S.S. [42]. A spectral

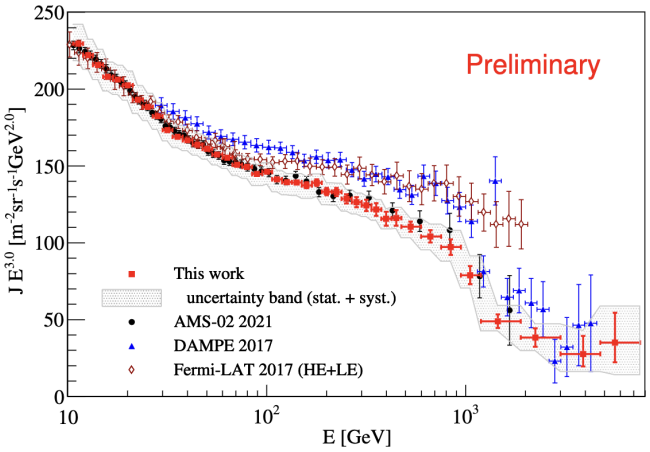

Figure 12: Cosmic ray electron spectrum as measured by various instruments, including CALET (red data points). Figure from [19].

steepening (a break) is observed at a particle energy of about 1 TeV. Beyond that the spectrum continues as a power law in the H.E.S.S. energy domain. This is the most prominent feature observed in cosmic ray spectra.

Electrons of energies exceeding 1 TeV lose rapidly energy due to synchrotron and inverse Compton radiation in the interstellar magnetic and radiation fields in a time $\lesssim 10^5$ yr. The synchrotron loss time further decreases at larger energies as $1/E$. A consequence of that, noticed already in [43], is that the very high energy electrons observed at the Earth must originate from young (age smaller than the electron energy loss time) and nearby accelerators, located within a diffusion length of the order of $\sqrt{6\,D\,t_a} \approx 4\times10^2 (D/10^{29}\mathrm{cm}^2/\mathrm{s})^{1/2}(t_a/10^5\mathrm{yr})^{1/2}$ pc, where D is the cosmic ray diffusion coefficient and t_a the age of the source (how long ago cosmic ray electrons were released in the interstellar medium). Therefore, depending on the adopted value of the cosmic ray diffusion coefficient and on the spatial density of cosmic ray sources, scenarios can be envisaged where multi-TeV electrons are mostly produced by a single (or very few) source(s) [44], or by many sources [45]. Unfortunately, it is not even clear whether cosmic ray nuclei and electrons originate from the same sources or not, and therefore the problem is still open.

Further puzzling behaviours have been found in the spectra of cosmic ray antiparticles. The excess in the anti-proton/proton ratio with respect to the predictions of standard transport models (left panel of Fig. 13) let to the speculation on the existence of a primary component of anti-protons. On the other hand, the same rigidity dependence observed in the spectra of anti-protons and positrons (and protons as well, but they are not shown in the right panel of Fig. 13) has been sometimes quoted in support of a secondary origin of both particles (though this would require non-standard scenarios for cosmic ray transport in the Galaxy see e.g. references in [2]). However, a model based on cosmic ray self-confinement (streaming instability) has been shown to provide a good fit to data without invoking a primary component of anti-protons [40].

One can see from Fig. 13 that while the measurements of the spectrum of positrons extends up to an energy of roughly 1 TeV, the spectrum of anti-protons is known up to an energy a factor of a few smaller. Extending the measurements of the spectrum of anti-protons to larger energies is

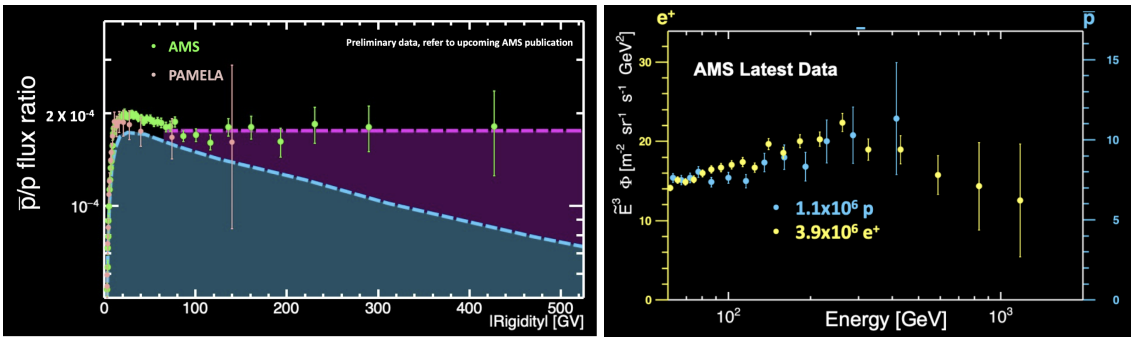

Figure 13: Left: Cosmic ray anti-proton/proton ratio as measured by AMS-02 and PAMELA. Figure from [46]. **Right:** Cosmic ray anti-protons and positrons spectra. Figure from [18].

important to probe to which extent the similar rigidity dependence persists.

5. Low energies

As cosmic ray spectra of all species are invariably steep, most particles are found in the low energy domain (broadly defined here as the MeV domain or below). This is then the energy domain which determines the abundance of different cosmic ray species (see e.g. [48]). Low energy cosmic rays are also studied by astronomers, as they play a key role in regulating the dense and cold phase of the interstellar medium. They are the only ionising agents able to penetrate large column densities of gas (UV photons are more easily absorbed), and therefore they set the ionisation and the heating rate in the interior of molecular clouds (for a review see [47]). This in turn determines the level of coupling between gas and magnetic field and regulates the cloud dynamics, impacting on the process of star and planet formation.

The ionisation rate inside interstellar clouds can be measured by means of observations of molecular lines, such has those of protonated molecular Hydrogen, H_3^+, which are observed as absorption lines in the infrared spectrum of background stars which happen to be locate behind (or inside) molecular clouds. This is because H_3^+ is formed following the ionisation by low energy cosmic rays of molecular Hydrogen, in a very fast ion-neutral reaction ($H_2^+ + H_2 \rightarrow H_3^+ + H$). In diffuse clouds, H_3^+ is destroyed due to dissociative recombination. The simplicity of the reaction network that determines the abundance of H_3^+ in interstellar clouds makes it an ideal tracer of the cosmic ray ionisation rate [49].

A puzzling outcome of observations is the fact that the ionisation rates derived by the measured abundances of H_3^+ are much larger (a factor of 10-100) than what is expected based on the observed *local* spectra of cosmic rays (obtained combining Voyager and AMS-02 data). This could be due to the existence of large spatial fluctuations in the intensity of MeV cosmic rays (the most effective ionising particles). The fluctuations are indeed expected, as cosmic rays are believed to be accelerated at discrete and stochastic sources (the remnants of supernova explosions). This, combined with the fact that MeV particles lose rapidly energy in the interstellar medium due to ionisation or Coulomb losses, might induce both spatial and temporal fluctuations in the intensity of low energy cosmic rays. In other words, the intensity of low energy cosmic rays will be large

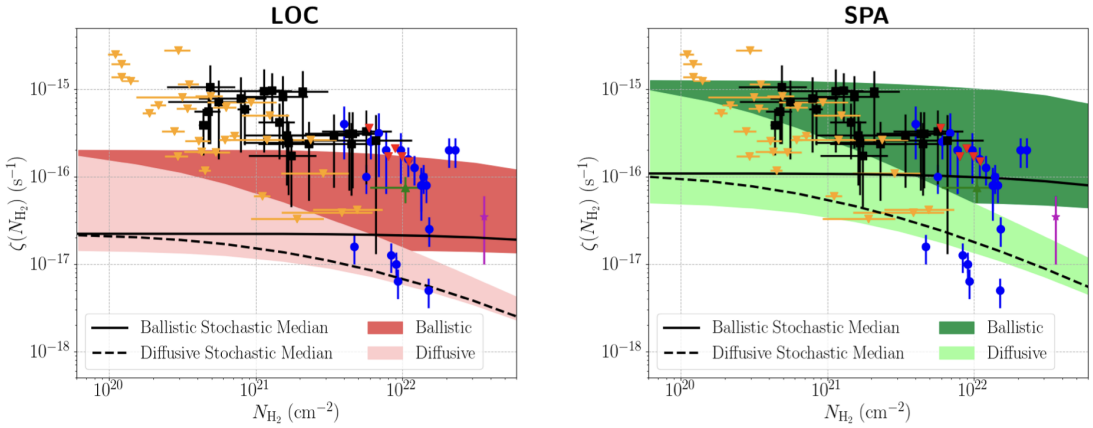

Figure 14: Cosmic ray ionisation rate inside molecular clouds as a function of the cloud column density. Available data points and upper limits are compared with model predictions for a ballistic and diffusive transport model for cosmic rays. Predictions are shown for clouds located in an interarm (left panel) and spiral arm (right panel) region. Figure from [50].

(smaller) at locations which are closer (farther away) from supernova remnants that released MeV particles in recent times.

The magnitude of this effect is shown in Fig. 14 (from [50]), where the measurements of the cosmic ray ionisation rate in a number of interstellar clouds are compared with predictions from models. Predictions are based on the assumption that cosmic rays (both nuclei and electrons) originate in supernova remnants (whose spatial distribution and explosion rate is known). Many different realisations of the Galaxy have been simulated. A Monte Carlo has been adopted to simulate the position and time of supernova explosions, and thenthe transport of cosmic rays in the interstellar magnetic field and into clouds has been modelled. The dashed and solid lines show the ionisation rates predicted using the median cosmic ray intensities computed in this way, while the shaded regions show the 95% uncertainty bands. Both a ballistic (straigth-line-propagation) and a diffusive model have been considered to describe the transport of cosmic ray *inside* interstellar clouds (while outside them the normal diffusion/advection Galactic transport has been adopted). Predictions have been made for an inter-arm (local) region (left panel in the figure) and spiral arm region (right panel). The number of cosmic ray sources is larger inside spiral arms, and this explains why predicted cosmic ray ionisation rates are larger in the right panel of Fig. 14. The presence of spatial fluctuations might dramatically reduce the disagreement between data and expectations (and also imply that the Solar system is located in a region where the cosmic ray ionisation rate is quite small).

Observations of H_3^+ spectral lines have also been performed in the Galactic centre region, and in particular in the Central Molecular Zone, the most massive molecular cloud complex in the Galaxy, located in the inner $\sim$ 100 pc of the disk. Results from such observations are even more puzzling, as the derived cosmic ray ionisation rates are in this case three to four orders of magnitude larger than expectations based on the local observed cosmic ray spectra (see [47] for a review).

The intensity of comic rays in the Central Molecular Zone can be inferred from gamma ray

observations. In order to explain the very large values of the ionisation rates without overshooting the gamma-ray emission, one is forced to postulate the existence of an "hidden" population of cosmic rays. The energy spectrum of such cosmic rays will have to be very steep, in order to have plenty of ionising ($\approx$ MeV) cosmic rays and not too many cosmic rays able to produce gamma rays. The problem with this scenario is that MeV cosmic rays cool very fast due to ionisation losses in the very dense gas that constitutes the Central Molecular Zone. Cosmic rays of lower energy cool even faster. Therefore, the effect of severe energy losses must be compensated by the acceleration of many particles. This makes the required energy budget unreasonably large. In order to sustain the hidden cosmic ray component at the level required to explain the measured ionisation rate, such particles should be continuously injected inside the Central Molecular Zone at a rate of $\approx 10^{40}$ erg/s. This is indeed a very large power, corresponding to about 10% of the total power of cosmic ray sources in the entire Galaxy. This very large amount of energy should be injected in a very small region (the inner 100 pc of the Galaxy) and should be visible uniquely through its effect on the gas ionisation rate. This seems a quite unreasonable scenario, and led to the conclusion that most likely competing ionising agents, such as UV and/or X-ray photons, must play a main role in ionising the gas in the Central Molecular Zone [51].

Finally, measurements of low energy cosmic rays are used to determine the chemical abundance of cosmic particles. It is a very well known fact that the composition of cosmic rays differs from that of the Solar system (which is often adopted as a proxy for interstellar composition). In fact, the composition of cosmic rays can be better reproduced assuming that they are accelerated out of a mixture of interstellar matter and massive star material, the stellar component being comparatively smaller [52] (see also [53]).

There are two ways to explain that, and both rely on the assumption that most cosmic rays originate from stellar clusters. Indeed, most stars form in clusters. The most massive among them blow very powerful winds, and eventually explode as supernovae. As a result of the combined effect of stellar winds and explosions, large cavities are inflated around clusters. Such cavities are called superbubbles. The diffuse gas present inside superbubbles is a mixture of interstellar and massive star material. Therefore, the shocks resulting from supernova explosions sweep and accelerate particles with a mixed (interstellar plus stellar) composition (see e.g. [54] and references therein). However, another scenario has been shown to provide a better fit to data [48]. In this scenario, cosmic rays are accelerated not only at supernova remnant shocks but also at the wind termination shocks that form around stars, and this explains the mixed composition of such particles.

In fact, the acceleration of particles at stellar winds termination shocks was already investigated in the early eighties in a number of pioneer papers and was found to be a possible solution to the problem of isotopic anomalies observed in the composition of cosmic rays [55]. In recent times, the detection of gamma-rays from a number of stellar clusters revived the interest in such objects as particle accelerators (see e.g. [56] and references therein). A model for particle acceleration at the collective wind termination shock that is expected to form around star clusters (and not individual stars) has been presented in [57].

6. ...and everything else

A large number of other topics were discussed during the conference. A brief list of selected contributions is provided below.

1. Theoretical studies on the formation of the Galactic cosmic ray halo [30, 58], and simulation of particle acceleration at shocks [59] and of particle transport in turbulent magnetic fields [60].

2. Accurate measurements of cross sections performed at the NA61/SHINE facility at CERN [61] (but see also [62, 63]).

3. Presentation/discussion of a number of future missions devoted to cosmic ray measurements and more.

   (a) The Trans-Iron Galactic Element Recorder for the International Space Station (TIGERISS) will measure the intensity of ultra heavy cosmic rays (planned launch date: 2026) [64].

   (b) The High Energy cosmic-Radiation Detection facility (HERD) will be installed on the China Space Station with the aim of performing the first direct measurements of cosmic rays up to the energies of the knee (the beginning of operations is expected to take place in 2027) [65].

   (c) The High Energy Light Isotope eXperiment (HELIX), a balloon-borne instrument, will measure the chemical and isotopic abundance of light cosmic rays, most notably the abundance of ^{10}Be (first long duration flight expected in 2024) [66].

   (d) The X-Ray Imaging and Spectroscopy Mission (XRISM) will measure the thermal emission from supernova remnants and possibly constrain the cosmic ray acceleration efficiency in such objects (launched shortly after the end of ICRC2023!) [67].

4. A number of presentations at the interface between the Cosmic Ray Physics (Direct, CRD) and Solar/Heliospheric Physics (SH) sessions [68–73].

5. Finally, it is somewhat surprising that none of the oral contributions was devoted to studies of the cosmic ray anisotropies. See however the poster presentations [74, 75].

7. Conclusions

Some years ago (in 2019, so about two ICRCs ago), together with some colleagues, we identified a number of open issues in cosmic ray physics [2]. It is interesting to see how many of those have been solved and how many still do not have an answer.

First of all, we now know that the cosmic ray spectrum is even more structured than we thought. In 2019, the hardening observed in the spectra of nuclei at ~200 GV was known, but not the softening at 10 TV. While we now know that the hardening is due to a variation of the rigidity dependence of the cosmic ray diffusion coefficient, we still don't know why spectra steepens at 10 TV.

Despite many proposals have been advanced, it is still not clear (as in 2019) why cosmic ray proton and Helium nuclei have different spectra, which is the origin of the prominent break observed at 1 TeV in the electron spectrum, and why protons, positrons, and anti-protons have roughly the same spectra.

The origin of the positron excess is still debated. However we know now that it is of paramount importance to extend measurements to large particle energies, in order to know whether the peak visible in Fig. 11 is due to a spectral cutoff or a break. In the former case, a dark matter origin of positrons would be favoured, while in the latter a pulsar origin would better fit data.

Finally, gamma-ray observations of star clusters revived the idea that this class of sources might contribute significantly to the intensity of cosmic rays. There is little doubt that the study of these objects will be central in future research on cosmic rays.

In conclusion, we keep advancing, slowly but steadily, towards a better comprehension of the origin and behaviour of Galactic cosmic rays.

Acknowledgments

I would like to thank the organisers of the 38th International Cosmic Ray Cconference for their invitation. Discussions I had during and after the conference with E. Amato, F. Donato, C. Evoli, A. Ivlev, G. Morlino, P. Mertsch, M. Paniccia, and A. Oliva helped me a lot in preparing my talk and this article. I also acknowledge support from Agence Nationale de la Recherche (project CRitiLISM, ANR-21-CE31-0028).

References

[1] A. M. Hillas, *Can diffusive shock acceleration in supernova remnants account for high-energy galactic cosmic rays?*, *J Phys G: Nucl Part Phys* **31** (2005) R95

[2] S. Gabici, C. Evoli, D. Gaggero, P. Lipari, P. Mertsch, E. Orlando, A. Strong, A. Vittino, *The origin of Galactic cosmic rays: Challenges to the standard paradigm*, *Int J Mod Phys D* **28** (2019) 1930022-339

[3] R. D. Blandford, P. Simeon, N. Globus, P. Mukhopadhyay, E. Peretti, K. Barrow, C. Kim, *A Hierarchical Framework for Explaining the Cosmic Ray Spectrum using Diffusive Shock Acceleration*, *PoS(ICRC2023)* **444** (2023) id.127

[4] O. Adriani, *et al.*, *The PAMELA Mission: Heralding a new era in precision cosmic ray physics*, *Phys Rep* **544** (2014) 323

[5] W. Xu, *Twelve Years of AMS on ISS*, *PoS(ICRC2023)* **444** (2023) id.007

[6] S. Torii, *Highlights from the CALET observations for 7.5 years on the International Space Station*, *PoS(ICRC2023)* **444** (2023) id.002

[7] A. Tykhonov, *DArk Matter Particle Explorer: 7 years in Space*, *PoS(ICRC2023)* **444** (2023) id.003

[8] K. Sakai, *et al.*, *Preliminary elemental spectra from protons to iron nuclei with ISS-CREAM*, *PoS(ICRC2023)* **444** (2023) id.136

[9] K. Kobayashi, P. S. Marocchesi, *Observation of spectral structures in the flux of cosmic ray protons with CALET on the International Space Station*, *PoS(ICRC2023)* **444** (2023) id.092

[10] A. Ruina, P. Coppin, A. Kotenko, P.-X. Ma, M. Stolpowskiy, A. Tikhonov, *Analysis of Individual Cosmic-Ray Proton and Helium Fluxes towards PeV Energies with DAMPE*, *PoS(ICRC2023)* **444** (2023) id.170

[11] A. Oliva, *Properties of Primary Cosmic Ray Nuclei: Eleven-year Results from the Alpha Magnetic Spectrometer*, *PoS(ICRC2023)* **444** (2023) id.086

[12] P. Brogi, K. Kobayashi, *Helium flux and its ratio to proton flux in cosmic rays measured with CALET on the International Space Station*, *PoS(ICRC2023)* **444** (2023) id.054

[13] C. Checchia, F. Stolzi, *Flux ratios of primary elements measured by CALET on the International Space Station*, *PoS(ICRC2023)* **444** (2023) id.093

[14] Y. Wei, C. Yue, D. Kyratzis, F. Barbato, M. Stolpowskiy, *Cosmic Ray Carbon and Oxygen Flux Measurements with the DAMPE Experiment*, *PoS(ICRC2023)* **444** (2023) id.165

[15] Q. Yan, V. Choutko, *Properties of Secondary Cosmic Ray Nuclei: Eleven-year Results from the Alpha Magnetic Spectrometer*, *PoS(ICRC2023)* **444** (2023) id.078

[16] V. Choutko, *Properties of Cosmic Sulfur and Determination of the Composition of Primary Cosmic Ray Carbon, Neon, Magnesium, and Sulfur: Results from the Alpha Magnetic Spectrometer*, *PoS(ICRC2023)* **444** (2023) id.060

[17] Y. Chen, *Properties of Third Group of Cosmic Nuclei: Results from the Alpha Magnetic Spectrometer*, *PoS(ICRC2023)* **444** (2023) id.096

[18] A. Kounine, *Understanding the Origin of Cosmic-Ray Electrons*, *PoS(ICRC2023)* **444** (2023) id.065

[19] Y. Akaike, S. Torii, *The cosmic-ray electron and positron spectrum measured with CALET on the International Space Station*, *PoS(ICRC2023)* **444** (2023) id.071

[20] DAMPE Coll., *Measurements of the boron-to-carbon and boron-to-oxygen flux ratios in cosmic rays with DAMPE*, *PoS(ICRC2023)* **444** (2023) id.159

[21] P. Maestro, Y. Akaike, *Boron flux in cosmic rays and its flux ratio to primary species measured with CALET on the International Space Station*, *PoS(ICRC2023)* **444** (2023) id.058

[22] J. Wei, *Cosmic-Ray Lithium and Beryllium Isotopes with the Alpha Magnetic Spectrometer*, *PoS(ICRC2023)* **444** (2023) id.077

[23] I.V. Moskalenko, *Modeling of Galactic cosmic rays and interpretation of direct measurements*, *PoS(ICRC2023)* **444** (2023) id.020

[24] A. Parenti, et al., *Analysis of cosmic lithium, beryllium and boron with the DAMPE space mission PoS(ICRC2023)* **444** (2023) id.137

[25] A.J. Farmer, P. Goldreich, *Wave Damping by Magnetohydrodynamic Turbulence and Its Effect on Cosmic-Ray Propagation in the Interstellar Medium* , *ApJ* **604** (2004) 671

[26] D.G. Wentzel, *Cosmic-ray propagation in the Galaxy: collective effects*, *ARA&A* **12** (1974) 71

[27] G.H. Choi, E.S. Seo, *Measurement of cosmic-ray proton and helium spectra from the ISS-CREAM experiment*, *PoS(ICRC2023)* **444** (2023) id.108

[28] M.A. Malkov, P.H. Diamond, M. Cao, I.V. Moskalenko, *On Why the 10-TeV Cosmic Ray Bump Originates in the Local Interstellar Medium*, *PoS(ICRC2023)* **444** (2023) id.143

[29] S.F. Kamijima, Y. Ohira, *Cosmic-ray acceleration in a supernova remnant shock propagating in a stellar wind with a wind termination shock*, *PoS(ICRC2023)* **444** (2023) id.109

[30] A. Ivlev, *Formation of the cosmic-ray halo: The role of nonlinear Landau damping*, *PoS(ICRC2023)* **444** (2023) id.048

[31] P.J. Deca, R. Kissmann, L. Einkemmer, *Efficient numerical methods for Anisotropic Diffusion of Galactic Cosmic Rays*, *PoS(ICRC2023)* **444** (2023) id.040

[32] I.V. Moskalenko, T.A. Porter, G. Jóhannesson, *The GALPROP cosmic ray and non-thermal photon emissions framework: v57 release*, *PoS(ICRC2023)* **444** (2023) id.041

[33] C. Evoli, G. Morlino, P. Blasi, R. Aloisio, *AMS-02 beryllium data and its implication for cosmic ray transport*, *Phys Rev D* **101** (2020) 023013

[34] H. Jacobs, P. Mertsch, V.H.M. Phan, *Unstable cosmic-ray nuclei constrain low-diffusion zones in the galactic disk*, *PoS(ICRC2023)* **444** (2023) id.104; *Unstable cosmic ray nuclei constrain low-diffusion zones in the Galactic disc*, *MNRAS* **526** (2023) 160

[35] S. Recchia, et al., *Grammage of cosmic rays in the proximity of supernova remnants embedded in a partially ionized medium*, *A&A* **660** (2022) A57

[36] M.J. Boschini, et al., *Deciphering the Local Interstellar Spectra of Secondary Nuclei with the Galprop/Helmod Framework and a Hint for Primary Lithium in Cosmic Rays*, *ApJ* **889** (2020) 167

[37] D. Maurin, E. Ferronato Bueno, Y. Génolini, L. Derome, M. Vecchi, *The importance of Fe fragmentation for LiBeB analyses. Is a Li primary source needed to explain AMS-02 data?*, *A&A* **668** (2022) A7

[38] C. Delgado, *Precision Measurement of Cosmic Ray Deuterons with Alpha Magnetic Spectrometer*, *PoS(ICRC2023)* **444** (2023) id.079

[39] N. Masi, F. D'Angelo, *Spectra of He isotopes and the 3He/4He ratio*, *PoS(ICRC2023)* **444** (2023) id.074

[40] A. Cuoco, *Implications of AMS-02 nuclei spectra on our understanding of cosmic-ray diffusion in the Galaxy*, *PoS(ICRC2023)* **444** (2023) id.064

[41] A.K. Harding, R. Ramaty, *The Pulsar Contribution to Galactic Cosmic Ray Positrons*, *ICRC Proc.* **2** (1987) 92

[42] M. de Naurois, *The Very-High-Energy electron spectrum observed with H.E.S.S.*, *PoS(ICRC2023)* **444** (2023) id.261

[43] F.A. Aharonian, A.M. Atoyan, H.J. Völk, *High energy electrons and positrons in cosmic rays as an indicator of the existence of a nearby cosmic tevatron*, *&A* **294** (1995) L41

[44] S. Recchia, S. Gabici, F.A. Aharonian, J. Vink, *Local fading accelerator and the origin of TeV cosmic ray electrons*, *Phys Rev D* **99** (2019) 103022

[45] C. Evoli, E. Amato, P. Blasi, R. Aloisio, *Galactic factories of cosmic-ray electrons and positrons*, *Phys Rev D* **103** (2021) 083010

[46] Z. Weng, *Antiproton Flux and Properties of Elementary Particle Fluxes in Primary Cosmic Rays Measured with the Alpha Magnetic Spectrometer on the ISS*, *PoS(ICRC2023)* **444** (2023) id.1403

[47] S. Gabici, *Low-energy cosmic rays: regulators of the dense interstellar medium*, *A&A Rev* **30** (2022) 4

[48] V. Tatischeff, J.C. Raymond, J. Duprat, S. Gabici, S. Recchia, *The origin of Galactic cosmic rays as revealed by their composition*, *MNRAS* **508** (2021) 1321

[49] S. Miller, J. Tennyson, T.R. Geballe, T. Stallard, *Thirty years of H_3^+ astronomy*, *Rev Mod Phys* **92** (2020) 035003

[50] V.H.M. Phan, P. Mertsch, S. Recchia, S. Gabici, *Stochasticity of cosmic rays from supernova remnants and the ionisation rates in molecular clouds*, *PoS(ICRC2023)* **444** (2023) id.076

[51] S. Ravikularaman, V.H.M. Phan, S. Gabici, *Cosmic rays and the high ionisation rates in the Galactic Centre*, *PoS(ICRC2023)* **444** (2023) id.046

[52] N.E. Walsh, *SuperTIGER Abundances of Galactic Cosmic Rays for the Atomic Number (Z) Interval 40 to 56*, *PoS(ICRC2023)* **444** (2023) id.053

[53] W.V. Zober, B.F. Rauch, *Results of the Ultra-Heavy Cosmic-Ray Analysis with CALET on the International Space Station*, *PoS(ICRC2023)* **444** (2023) id.088

[54] R. Lingenfelter, *Cosmic rays from supernova remnants and superbubbles*, *Adv Space Res* **62** (2018) 2750

[55] M. Cassé, J. Paul, *Local gamma rays and cosmic-ray acceleration by supersonic stellar winds*, *ApJ* **237** (1980) 236; *On the stellar origin of the ^{22}Ne excess in cosmic rays*, *ApJ* **258** (1982) 860; C.J. Cesarsky, T. Montmerle, *Gamma-Rays from Active Regions in the Galaxy - the Possible Contribution of Stellar Winds*, *Space Sci Rev* **36** (1983) 173

[56] S. Gabici, *Star clusters as cosmic ray accelerators*, *to appear on the Proceedings of GAMMA2022*, arXiv:2301.06505

[57] G. Morlino, S. Menchiari, E. Amato, N. Bucciantini, *Contribution to Galactic cosmic rays from young stellar clusters*, *PoS(ICRC2023)* **444** (2023) id.157

[58] B. Schroer, D. Caprioli, P. Blasi, *Implications of cosmic-ray self-confinement in the Galaxy*, *PoS(ICRC2023)* **444** (2023) id.124

[59] E. Simon, D. Caprioli, C. Haggerty, B. Reville, *Maximum energy achievable in supernova remnants: self-consistent simulations*, *PoS(ICRC2023)* **444** (2023) id.150

[60] M. Kuhlen, P. Mertsch, V.H.M. Phan, *From test particle simulations to cosmic-ray transport*, *PoS(ICRC2023)* **444** (2023) id.146

[61] N. Amin, *Pilot Study on the Measurement of the Production of Boron Isotopes in C+p Reactions at 13.5A GeV/c with NA61/SHINE*, *PoS(ICRC2023)* **444** (2023) id.075

[62] P. Coppin, A. Tykhonov, A. Kotenko, A. Ruina, M. Stolpowsky, *Probing hadronic cross sections in the TeV - PeV regime with DAMPE through machine learning techniques*, *PoS(ICRC2023)* **444** (2023) id.142

[63] P. Ghosh, et al., *Isotopic Production Cross Section Updates in GALPROP for Supporting TIGERISS*, *PoS(ICRC2023)* **444** (2023) id.049

[64] B.F. Rauch, W.V. Zober, *The Trans-Iron Galactic Element Recorder for the International Space Station (TIGERISS)*, *PoS(ICRC2023)* **444** (2023) id.171

[65] Z. Wang, *Introduction of the HERD experiment onboard the China Space Station PoS(ICRC2023)*, **444** (2023) id.181

[66] S.P. Wakely, et al., *Cosmic-ray Isotope Measurements with HELIX PoS(ICRC2023)*, **444** (2023) id.118

[67] J. Shimoda, *Ion Heating Mechanism & Cosmic Ray Production in Collisionless Shocks*, *PoS(ICRC2023)* **444** (2023) id.052

[68] A. Sotgiu, B/ Panico, *Galactic Cosmic Ray Observations with the High Energy Particle Detector (HEPD-01) on board the CSES-01 Satellite*, *PoS(ICRC2023)* **444** (2023) id.114

[69] Y. Jia, *Precision Measurement of Daily Proton and Helium Fluxes by the Alpha Magnetic Spectrometer*, *PoS(ICRC2023)* **444** (2023) id.073

[70] Z. Tang, *Time variations of the Antiproton Fluxes over a Solar Cycle: Results from the Alpha Magnetic Spectrometer on the ISS*, *PoS(ICRC2023)* **444** (2023) id.133

[71] T. Su, *Temporal Structures in Positron Spectra and Charge Sign Effects in Galactic Cosmic Rays*, *PoS(ICRC2023)* **444** (2023) id.091

[72] Z. Li, *Temporal Structures of Cosmic Elementary Particles*, *PoS(ICRC2023)* **444** (2023) id.177

[73] V. Formato, A.R. Conde, *Precision Measurement of the Monthly Light Ion Fluxes in Cosmic Rays with the Alpha Magnetic Spectrometer on the International Space Station*, *PoS(ICRC2023)* **444** (2023) id.084

[74] M.A. Velasco Frutos, *Anisotropy of Cosmic Elementary particles measured with the Alpha Magnetic Spectrometer on the ISS*, *PoS(ICRC2023)* **444** (2023) id.081

[75] S. Lei, *Studies of Cosmic Ray Anisotropies with DAMPE*, *PoS(ICRC2023)* **444** (2023) id.152